

# Ultra-Bright Stimuli-Responsive Photonic Crystals for High-Performance Anticounterfeiting Coatings

Ziqiang Tian, Jinyao Zhu, Qilin Guo, Lulu Chen, Jia Guo, and Changchun Wang\*

Photonic crystals (PCs) with unique light manipulation capability have attracted widespread attentions. However, weak photonic bandgaps, poor structural color saturation, and tedious preparation process restrict their further development and practical application. Herein, an ultra-bright stimuli-responsive PC film with excellent optical performance is prepared by assembly of cadmium sulfide@polyacrylic acid (CdS@PAA) core-shell nanoparticles into PCs through molecule-mediated shearing-induced assembly technique (MSAT), this fabrication process is fast and facile, the solid periodic micro/nano-structures can be formed within 10 s, and a wide selection range of structural color can be obtained. The high refractive index of CdS guarantees high brightness of the PC films. The prerequisite of using MSAT for preparation of large-sized ultra-bright PC film is that the CdS@PAA nanoparticles possess appropriate thickness of PAA shell. Compared with conventional PCs, the ultra-bright PC films present strong photonic bandgaps and high structural color saturation, the relative reflectance is up to 130% compared with a standard aluminum mirror, which is more than four times reflectivity of PS@PAA microspheres. In addition, the PC paint is prepared by mashing the ultra-bright PC film and blending it with transparent polydimethylsiloxane (PDMS) matrix, the PC coating prepared by alkali treated ultra-bright PC pigments can achieve good water response ability and anticounterfeiting effect.

public traffic system, certain colors are used by many well-known brands as their signature colors and so on. Humanity's fascination and exploration of color have never ceased for thousands of years. Usually, colors are classified into chemical color and structural color based on the principle of color generation.<sup>[1]</sup> Chemical color, also known as pigmentary color, is generated by absorbing specific wavelengths of light through certain compounds and reflecting other wavelengths of light. Structural color, also known as physical color, originate from complicated interaction between light and periodic micro/nano-structures of matter, such as diffraction, refraction, and interference.<sup>[2]</sup> They have been broadly applied in the fields of display technology,<sup>[3]</sup> anticounterfeit labels,<sup>[4]</sup> and decorative materials.<sup>[5]</sup> Compared with the chemical color, the structural color is generally more stable, and less prone to fade under chemical reactions and surrounding changes.<sup>[6]</sup> Besides, the structural color possesses many intrinsic merits including environmental protection, antiphotobleaching, and iridescent effect.<sup>[7]</sup>

Inspired by organisms with periodic micro/nano-structures yielding structural color in nature, such as chameleon's skin, peacock's feather, and butterfly's wing, people constructed artificial periodic crystalline materials that exhibit structural colors and named photonic crystals (PCs).<sup>[8]</sup> PCs are constructed from two or more media with different refractive indices or dielectric constants, and these media are periodically arranged into highly ordered structures in space.<sup>[9]</sup> The most conspicuous characteristic of PCs is their photonic bandgap (PBG).<sup>[10]</sup> The PBG empowers PCs to redistribute the density of the optical state, which is specifically manifested by prohibiting the propagation of incident light with specific wavelengths within the PBG range through PCs and reflecting the light.<sup>[11]</sup> When the PBG is within the visible region, coherent diffraction is generated between the prohibited light with the corresponding wavelength and PCs with periodically ordered structures. Eventually, the artificial PCs show structural colors observed by human eyes.<sup>[12]</sup> In addition, the structural color of PCs can be regulated based on Bragg's law.<sup>[13]</sup> Considering the outstanding light-manipulation capacity and unique iridescent effect of PCs, persistent endeavors are being put into the optics-related applications of

## 1. Introduction

Color plays many extremely significant roles in nature and human society. For example, chameleons and lizards camouflage themselves by changing their skin colors to evade the predation of natural enemies, peacock attracts the opposite sex by the bright colors in their tail feathers. In human society, color is also more widely used, vivid visual effect through combinations and contrasts of colors is created by artists, different colors are used to indicate directions and warning signals in

Z. Tian, J. Zhu, Q. Guo, L. Chen, J. Guo, C. Wang  
State Key Laboratory of Molecular Engineering of Polymers  
Department of Macromolecular Science  
Laboratory of Advanced Materials  
Fudan University  
Shanghai 200433, China  
E-mail: cawang@fudan.edu.cn

The ORCID identification number(s) for the author(s) of this article can be found under <https://doi.org/10.1002/adom.202402776>

DOI: 10.1002/adom.202402776

structural colors in realms of photonic pigments,<sup>[14]</sup> information securities,<sup>[15]</sup> encryption-decryption,<sup>[16]</sup> colorimetric physical/chemical sensors,<sup>[17]</sup> color displays,<sup>[18]</sup> visual detections,<sup>[19]</sup> photonic printings,<sup>[20]</sup> smart windows,<sup>[21]</sup> rewritable papers,<sup>[22]</sup> optical devices,<sup>[23]</sup> and lasers.<sup>[24]</sup>

Enhancing PBG (strengthening reflection intensity), improving structural color saturation, and creating more vibrant colors have always been the research focus for PCs. Based on previous studies,<sup>[25]</sup> the optical performance of PCs is highly dependent on the refractive index contrast ( $\Delta n$ ) between the assembly units and the surrounding matrix. A larger  $\Delta n$  is capable of contributing more intense PBG, higher structural color saturation, and more vibrant colors. Therefore, selecting monodisperse nanoparticles with high refractive index as assembly units to construct PCs with large  $\Delta n$  is a desirable and effective strategy for fabricating brighter PCs. Currently, most conventional PCs are generally prepared through self-assembling SiO<sub>2</sub> nanoparticles in polymer matrix.<sup>[26]</sup> The refractive index of SiO<sub>2</sub> is only 1.46, which is similar to that of most polymer matrices (1.4–1.5), the small  $\Delta n$  (0.04–0.06) between SiO<sub>2</sub> nanoparticles and polymer matrices in conventional PC systems can only contribute to poor structural color saturation and weak reflection intensity (less than 30%). In response to the above issue, many research works have been developed. For example, Wu's group designed and fabricated non-close-packed (NCP) PC films by arranging ZnS nanoparticles with a high refractive index of 1.91 orderly inside polymers with a refractive index of 1.3–1.5 through a two-step filling method.<sup>[27]</sup> The large  $\Delta n$  (0.41–0.61) between ZnS nanoparticles and polymers enables the NCP PC film to display bright structural color with a reflection intensity of 45%. Ge et al. prepared electrically tunable liquid PCs by dispersing CeO<sub>2</sub>@SiO<sub>2</sub> nanoparticles (the refractive index of the CeO<sub>2</sub> is 2.20) in propylene carbonate with a refractive index of 1.59,<sup>[28]</sup> the relatively large  $\Delta n$  between CeO<sub>2</sub>@SiO<sub>2</sub> nanoparticles and propylene carbonate gives rise to highly saturated structural colors of the CeO<sub>2</sub>-based PCs. Although these research works have obtained remarkable progress, there is still much room for improvement in the structural color saturation and reflection intensity of PCs.

Cadmium sulfide (CdS) has a refractive index up to 2.51, which is higher than that of SiO<sub>2</sub> (1.46), PS (1.595), ZnS (1.91), and CeO<sub>2</sub> (2.20). CdS nanoparticles are increasingly becoming desirable assembly units to constructed PCs with excellent optical performances and have attracted widespread research enthusiasm in recent years.<sup>[29]</sup> However, developing a convenient and advanced technique for assembling CdS nanoparticles into PC structures with optimized efficiency and stable controllability is still a big challenge. Different from other nanoparticles, CdS nanoparticles present a strong intrinsic cadmium yellow, which not only seriously affects the structural color purity and saturation of CdS-based PCs, but also restricts their practical application. Therefore, the technique for assembling CdS nanoparticles into PC structures must provide very strong forces to ensure that the CdS nanoparticles are effectively arranged into highly ordered periodic arrays, so that the structural colors are capable of suppressing the strong intrinsic cadmium yellow of CdS nanoparticles. Recently, the shearing force has been proved as an effective driving force to assemble nanoparticles with large material density into highly ordered PC structures. For example, Su and his coworker<sup>[30]</sup> synthesized CdS@SiO<sub>2</sub>@P(MMA-

BA) core-shell microspheres and constructed the PC films with vivid structural colors through melt-compression. Once uniaxial compression at high temperature, the soft P(MMA-BA) polymer shells were merged into a continuous flowing polymer melt, generating strong shearing forces that drove the assembly of CdS@SiO<sub>2</sub> cores into ordered arrays. However, this strategy has drawbacks including tedious and complicated preparation procedures, thermal energy consumption, and limited production scale. These weaknesses restrict the practical application of PC materials to some extent. Therefore, developing a desirable technique for assembling CdS nanoparticles into PC structures is an urgent demand.

In this work, a new-type ultra-bright PC film is directly prepared by assembling the CdS@PAA core-shell nanoparticles into PC film through a distinctive high-throughput technique called molecule-mediated shearing-induced assembly technique (MSAT) at room temperature. The structural color and reflection intensity of the ultra-bright PC films can be precisely regulated by changing the particle size of the CdS cores and the cross-linking degree of the PAA shells, respectively. Compared with conventional PCs, these ultra-bright PC films exhibit evident advantages including strong photonic bandgaps (relative reflectance is up to 130%), fast and facile fabrication process (within 10 seconds), solid periodic micro/nano-structures, and a wide selection range of structural color. Based on these excellent advantages, a new kind of anticounterfeiting PC coatings is further exploited.

## 2. Results and Discussion

### 2.1. Syntheses of Monodisperse CdS and CdS@PAA Core-Shell Composite Nanoparticles

The step-by-step synthesis process of the monodisperse CdS and composite CdS@PAA core-shell nanoparticles was illustrated in **Figure 1a**. In the synthesis of the monodisperse CdS nanoparticles (the first step in **Figure 1a**), the thiourea (TU), cadmium nitrate tetrahydrate (Cd(NO<sub>3</sub>)<sub>2</sub>·4H<sub>2</sub>O), polyvinylpyrrolidone (PVP), and diethylene glycol (DEG) serve as sulfur source, cadmium source, polymeric surfactant, and reaction solvent, respectively. After reaction, the obtained product suspension presents a uniform intrinsic cadmium yellow color (**Figure 1b** inset), implying the successful synthesis of CdS nanoparticles. The collected CdS nanoparticles possess a regular spherical shape and high uniformity in size (**Figure 1b**), which is favorable for preparing PCs constructed using the obtained CdS nanoparticles as assembly units. The particle sizes of CdS nanoparticles can be well regulated by adjusting the amounts of TU and Cd(NO<sub>3</sub>)<sub>2</sub>·4H<sub>2</sub>O under their molar ratio kept at 1:1 (**Table S1**, Supporting Information). Here, the monodisperse CdS nanoparticles with a size range from 92 to 170 nm were selectively synthesized (**Figure S1**, Supporting Information). These CdS nanoparticles with different particle sizes have definite spherical shapes and narrow size distribution, showing great monodispersity. The X-ray diffraction (XRD) patterns of CdS nanoparticles with varying particle sizes display consistent peak positions and relative intensities of diffraction with the standard cubic CdS (**Figure S2**, Supporting Information), implying these collected CdS nanoparticles with different particle sizes are crystalline. These results suggest that CdS nanoparticles possess large dielectric constant and high refractive index

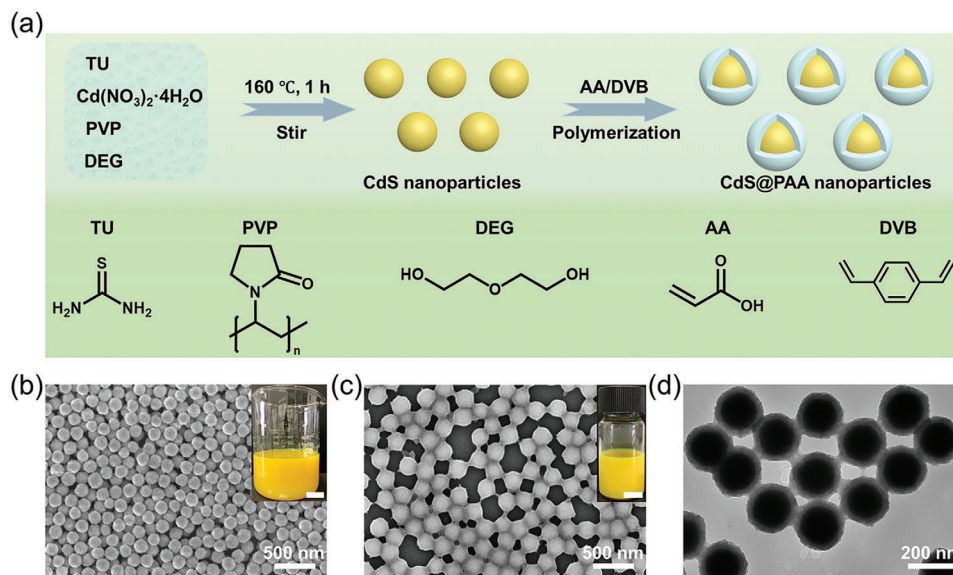


**Figure 1.** The preparation of CdS and CdS@PAA core–shell nanoparticles. a) Schematic illustration of the fabrication process of CdS and CdS@PAA nanoparticles. b) The scanning electron microscope (SEM) image of monodisperse CdS nanoparticles with a diameter of 170 nm. The inset photograph represents unwashed CdS nanoparticles in a mixture of ethanol and diethylene glycol. The scale bar is 2 cm. c) The SEM image of corresponding CdS@PAA nanoparticles. The inset photograph represents CdS@PAA nanoparticles dispersed in ethanol. The scale bar is 1 cm. d) The corresponding transmission electron microscope (TEM) image of the monodisperse CdS@PAA nanoparticles with a PAA shell thickness of  $\approx 32$  nm.

regardless of particle sizes. The regular spherical shape, adjustable particle sizes, narrow size distribution, and high refractive index make the CdS nanoparticles desirable assembly units for constructing ultra-bright PCs.

The CdS@PAA core–shell composite nanoparticles were synthesized through one-step reflux precipitation polymerization (ORPP) reaction (the second step in Figure 1a). Due to the strong hydrogen bonding between PAA and PVP and the excellent precipitation effect of PAA in acetonitrile, the CdS nanoparticles can be uniformly encapsulated by PAA shells without tedious surface modification, forming uniform CdS@PAA core–shell composite nanoparticles. The cross-linking degree of all the PAA shells is 25.9%. As shown in Figure 1c, no self-nucleation of PAA is observed after the polymerization, guaranteeing the monodispersity of the CdS@PAA nanoparticles. The CdS@PAA nanoparticles can be uniformly dispersed in ethanol and present intrinsic cadmium yellow (Figure 1c inset), intimating the polymerization does not affect the properties of CdS cores. Besides, the TEM image directly exhibits the well-defined core–shell structures of the CdS@PAA composite nanoparticles (Figure 1d). The PAA shell on the surface of each CdS core has a consistent thickness. This result further confirms that the regular spherical shape and monodispersity of nanoparticles are maintained after the encapsulation, which offers prerequisites for the construction of photonic structures using the CdS@PAA core–shell nanoparticles as assembly blocks.

The CdS and CdS@PAA nanoparticles display durable dispersion stability (Figure S3, Supporting Information). After the CdS/ethanol and CdS@PAA/ethanol suspensions were stood for a month, both suspensions still showed uniform intrinsic cadmium yellow without sedimentation and aggregation of nanoparticles. Meanwhile, the CdS@PAA core–shell composite nanoparticles exhibit excellent structural stability (Figure S4, Support-

ing Information). After being sonicated for different duration times, the CdS@PAA composite nanoparticles still maintained well-defined core–shell structures. This result proves that the PAA shell layers have been firmly anchored to the surface of CdS cores after RPP. The structural stability guarantees that the core–shell structures of composite CdS@PAA nanoparticles will not be damaged under subsequent shearing forces. According to the same recipe, all CdS nanoparticles with a size range from 92 to 170 nm were successfully capsulated with PAA shells with a thickness of  $\approx 32$  nm. Similarly, the resulting CdS@PAA nanoparticles with various sizes present uniform spherical shape and narrow size distribution (Figure S5, Supporting Information). Each CdS@PAA nanoparticle exhibited clear boundaries and well-defined core–shell structures regardless of particle size (Figure S6, Supporting Information).

## 2.2. Preparation and Characterizations of Ultra-Bright PC Films

The ultra-bright PC films were prepared through a distinctive high-throughput technique called the molecule-mediated shearing-induced assembly technique (MSAT) at room temperature (Figure 2a). The MSAT process was run by employing a machine called the open mill (Figure S7, Supporting Information). Briefly, the dry CdS@PAA core–shell composite nanoparticles with a particle size of about 199 nm were firstly blended with the mediator molecule acrylic acid (AA) through a strong stir. Due to AA having a similar solubility parameter with the PAA shell of CdS@PAA nanoparticles, the AA molecules can swell and soften PAA shells after stirring for a few minutes, and the soft PAA shells connect together in the mixture. As a result, the whole blending system formed a continuous phase called CdS@PAA-AA slurry with a certain viscosity. The CdS@PAA

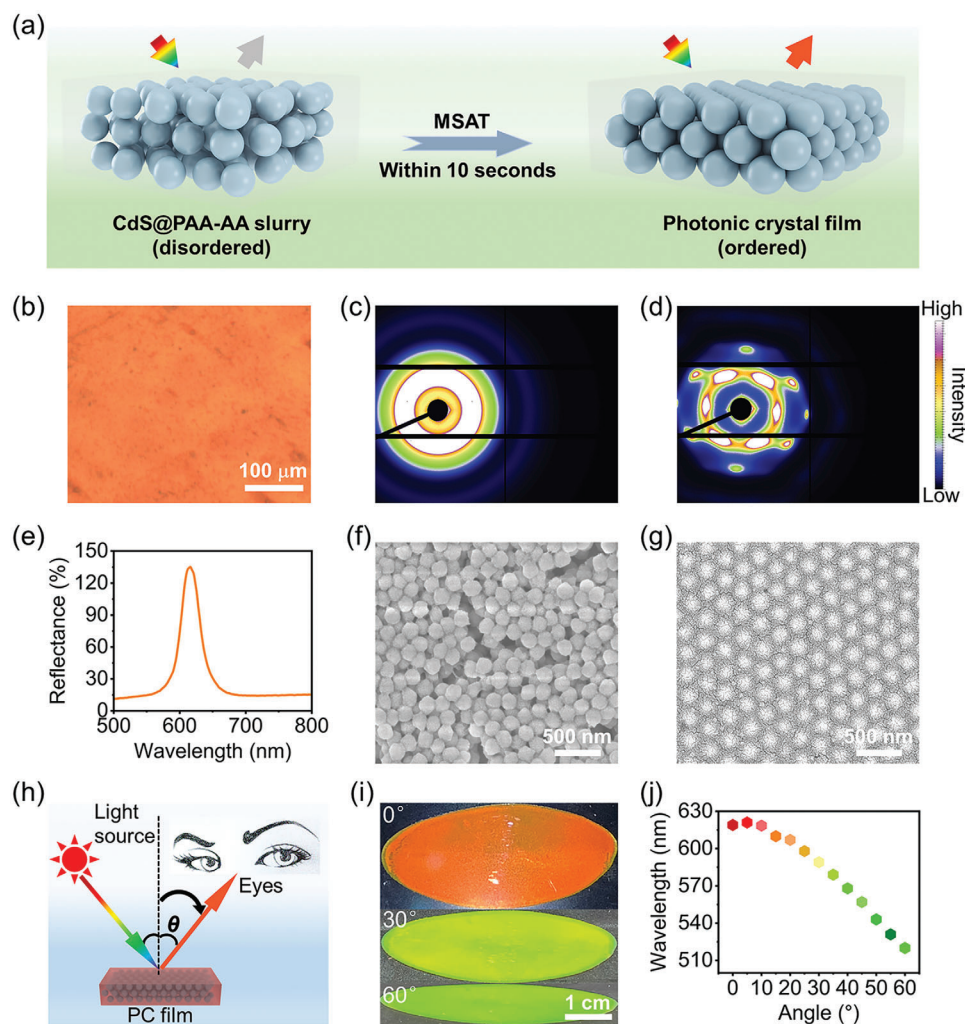


**Figure 2.** The fabrication and characterization of ultra-bright PC film. a) Schematic illustration of fabricating the ultra-bright PC film through the molecule-mediated shearing-induced assembly technique (MSAT). b) Optical microscope image of the ultra-bright PC film. The 2D ultras-small-angle X-ray scattering (USAXS) patterns of c) CdS@PAA-AA slurry and d) the ultra-bright PC film. e) The reflection spectrum of the ultra-bright PC film. The SEM images of f) CdS@PAA-AA slurry with disordered structures and g) the ultra-bright PC film with long-range ordered structures. h) Schematic illustration of the light reflection with different viewing angles on the ultra-bright PC film. i) Digital photographs of the ultra-bright PC film under different viewing angles. j) Relationship between reflection wavelength of the ultra-bright PC film and viewing angles ( $\theta$  increases from  $0^\circ$  to  $60^\circ$ , the intervals are  $5^\circ$ ).

nanoparticles in the CdS@PAA-AA slurry presented a disordered state with random arrangement. On the contrary, the CdS@PAA nanoparticles were arranged into periodic ordered arrays after MSAT. This is because the MSAT can provide a strong shearing force to drive the assembly of CdS@PAA nanoparticles into long-range ordered structures. The monodisperse CdS nanoparticles should be non-close-packed into PCs.<sup>[31]</sup> Finally, the ultra-bright PC films with about thickness of 57 μm were successfully prepared.

During the MSAT process, the AA molecules enhanced the interactions between nanoparticles, and the shearing force provided by MSAT could be effectively delivered to each CdS@PAA nanoparticle. As a result, the interconnected PAA shells radially move and drive all CdS@PAA nanoparticles to assemble into the ultra-bright PC films under the shearing force. After hot-curing, the periodically ordered structures of PC films were solidified.

The MSAT process of the CdS@PAA nanoparticles transforming from the disorder to the high order can be accomplished within 10 seconds, which tremendously improves the efficiency of the preparation of PCs compared to conventional evaporation-inducing strategies. Moreover, the large-area production of PC films can be achieved under the premise of ensuring sufficient slurry through the MSAT.<sup>[32]</sup>

The as-prepared ultra-bright PC film exhibits excellent optical properties. As shown in Figure 2b, The PC film presents an ultra-bright rufous structural color with high saturation suppressing the intrinsic cadmium yellow of CdS nanoparticles, the vivid structural color is uniform and consists of numerous micro-crystals. Different from the 2D USAXS pattern of the CdS@PAA-AA slurry displayed amorphous scattering rings (Figure 2c), the 2D USAXS pattern of the ultra-bright PC film illustrates clear and brilliant diffraction spots with high intensity on the outer

scattering ring (Figure 2d). This result demonstrates that the ultra-bright PC film possesses highly ordered PC structures run through the entire PC film from surface to interior. The reflection spectrum of the ultra-bright PC film exhibits a slender reflection peak located at 616 nm (Figure 2e), the reflection wavelength of the ultra-bright PC film agrees well with its structural color. The reflectance of the ultra-bright PC film is as high as 136%, which indicates that the brightness of the ultra-bright PC film surpasses the standard aluminum mirror. The high reflection intensity further proves the enhanced PBG and high structural color saturation of the ultra-bright PC film. Additionally, the microstructures can be directly observed by SEM images. Before MSAT, the microstructure of the slurry is disordered CdS@PAA nanoparticles with random arrangement (Figure 2f). After MSAT, the ultra-bright PC film presents a long-range order face-centered cubic microstructure of CdS@PAA nanoparticles (Figure 2g). The contrast explains the excellent optical properties of the ultra-bright PC film in terms of the structures.

The ultra-bright PC film also possesses stable iridescence effect. Due to the long-range ordered photonic structures, the structural colors of the ultra-bright PC films vary with the change of viewing angles. Figure 2h shows the angular dependence of structural color when viewed under sunlight, the  $\theta$  is the viewing angle, in the observing mode, the structural colors change from rufous to yellow to green as the  $\theta$  increases from  $0^\circ$  to  $60^\circ$  (Figure 2i). The corresponding reflection wavelength of the ultra-bright PC film blueshifts from 619 to 522 nm (Figure 2j). The original angle-resolved reflection spectra are illustrated in Figure S8 (Supporting Information), which evidently displays the angle-dependence property of the ultra-bright PC film. It's noteworthy that the ultra-bright PC film can maintain relatively high reflection intensities under various  $\theta$  than traditional PCs, implying a stable iridescence effect. This is because high refractive index of the assembly block CdS@PAA nanoparticles. Besides, the relationship between  $\theta$  and reflection wavelength can be precisely calculated by Bragg's diffraction formula (Equation (1)).

$$m\lambda = 1.633D(n_{\text{eff}}^2 - \sin^2\theta)^{1/2} \quad (1)$$

where,  $m$  denotes the Bragg diffraction order;  $\lambda$  represents the reflection wavelength of the ultra-bright PC film;  $D$  represents the interparticle spacing between neighboring nanoparticles;  $n_{\text{eff}}$  represents the effective refractive index of the ultra-bright PC film. The  $n_{\text{eff}}$  is calculated with Equation (2).

$$n_{\text{eff}}^2 = n_{\text{CdS@PAA}}^2 f_{\text{CdS@PAA}} + n_{\text{AA}}^2 f_{\text{AA}} \quad (2)$$

where,  $n_{\text{CdS@PAA}}$  and  $n_{\text{AA}}$  represent the refractive indices of the CdS@PAA and AA, respectively;  $f_{\text{CdS@PAA}}$  and  $f_{\text{AA}}$  represent the volume fractions of the CdS@PAA nanoparticles and AA in the ultra-bright PC film, respectively.

### 2.3. Necessary Conditions for Preparing the Ultra-Bright PC Film Through the MSAT

The slurry with appropriate viscosity and enhanced interaction between nanoparticles are necessary conditions for fabricating the ultra-bright PC film through the MSAT. The suitable viscosity of the CdS@PAA-AA slurry and the enhanced interaction

between the CdS@PAA nanoparticles are generally achieved by regulating the PAA shell thickness of the CdS@PAA core-shell composite nanoparticles. Herein, CdS nanoparticles with a particle size of  $\approx 115$  nm were selected and capsulated with PAA shells with different thicknesses of  $\approx 5$ , 16, and 32 nm (Figure 3a). After that, the pure CdS nanoparticles without the soft polymer shell and the obtained CdS@PAA nanoparticles with varying shell thicknesses were blended with mediator molecule AA and stirred, respectively (Figure 3b). According to our previous reports,<sup>[33]</sup> the volume fractions of different nanoparticles in their respective mixture systems were maintained at 33.3%. For the pure CdS nanoparticles (Figure 3a I), there was an obvious interface between nanoparticles and mediator molecule AA in the CdS-AA mixture (Figure 3b I). This result indicates that the CdS nanoparticles sediment in mixture and the AA molecules cannot swell into the CdS nanoparticle. The mixture system is not a continuous phase and fails to form a slurry. For the CdS@PAA nanoparticles with PAA shell thicknesses of 5, 16, and 32 nm, the three kinds of core-shell nanoparticles could be uniformly dispersed in AA to form continuous phases, respectively. The AA molecules swelled and softened the PAA shells to produce slurries with different viscosity, respectively (Figure 3b II, III, IV). The obtained CdS@PAA (32 nm shell)-AA slurry showed weak structural color. This color is more noticeable than that of the CdS@PAA (5 nm shell)-AA and the CdS@PAA(16 nm shell)-AA slurries, implying the CdS@PAA nanoparticles with a PAA shell thickness of 32 nm experienced stronger interparticle interaction than the CdS@PAA nanoparticles with shell thicknesses of 5 and 16 nm during stir.

The viscosity of slurries and interaction between nanoparticles can be precisely characterized by rheological results. With the PAA shell thicknesses of CdS@PAA nanoparticles increasing from 5 to 16 to 32 nm, the viscosities of the corresponding slurries fabricated from these CdS@PAA nanoparticles gradually increased (Figure S9, Supporting Information). Specially, when the shear rate is  $0.00911 \text{ s}^{-1}$ , the viscosities of the slurries increased from 65 390 to 77 690 to 116 700 Pa·s (Figure 3c). The raised viscosities facilitate the shearing force to be effectively delivered to each CdS@PAA nanoparticle and drive these CdS@PAA nanoparticles toward assembly. The storage moduli ( $G'$ ) and loss moduli ( $G''$ ) of the three kinds of slurries progressively increased as the PAA shell thicknesses increased from 5 to 16 to 32 nm (Figure 3d). This result indicates that the interactions between nanoparticles in slurries can be enhanced as shell thicknesses increase.

The CdS-AA mixture and the three kinds of CdS@PAA-AA slurries were implemented with the MSAT to prepare films, respectively (Figure 3e). For the CdS-AA mixture, the pure CdS nanoparticles generated persistent rigid collisions during MSAT. The shearing force cannot be transmitted to each CdS nanoparticle and effectively drives them to move radially. The pure CdS nanoparticle aggregates and AA liquid randomly dispersed between two PET films, yielding an uneven sheet-like CdS-AA mixture. The sheet-like CdS-AA mixture shows intrinsic cadmium yellow without structural color (Figure 3e I). Correspondingly, the SEM image directly shows that the pure CdS nanoparticles present chaotically packed aggregates in the CdS-AA mixture (Figure 3g). The CdS@PAA (5 nm shell)-AA and the CdS@PAA(16 nm shell)-AA slurries formed two

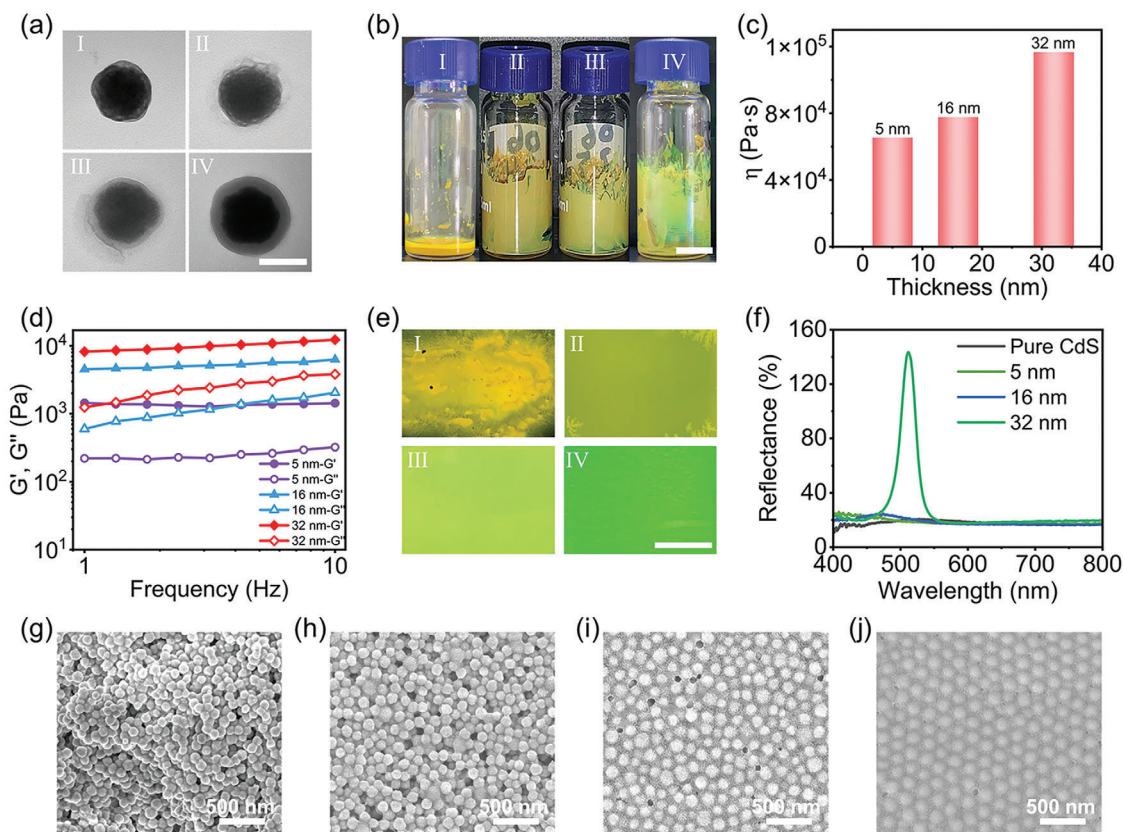


**Figure 3.** The influence of shell thicknesses of CdS@PAA nanoparticles on the preparation of ultra-bright PC film by MSAT. a) TEM images of (I) pure CdS and CdS@PAA nanoparticles with PAA shell thicknesses of (II) 5, (III) 16, and (IV) 32 nm, respectively. The scale bar is 100 nm. b) Digital photographs of (I) the mixture of pure CdS and AA and three slurries prepared by mixing AA and CdS@PAA nanoparticles with PAA shell thicknesses of (II) 5, (III) 16, and (IV) 32 nm, respectively. The scale bar is 5 mm. c) The viscosity of three slurries prepared from CdS@PAA nanoparticles with different PAA shell thicknesses (5, 16, and 32 nm) at the shear rate of  $0.00911 \text{ s}^{-1}$ . d) The storage modulus ( $G'$ ) and loss modulus ( $G''$ ) of the three slurries as a function of oscillatory frequency. e) Digital photographs and f) corresponding reflection spectra of (I) the mixture of pure CdS and AA as well as three films prepared by the three slurries with PAA shell thicknesses of (II) 5, (III) 16, and (IV) 32 nm after the MSAT, respectively. The scale bar is 1 cm. g) SEM image of the mixture of pure CdS and AA. h–j) SEM images of the three films prepared from CdS@PAA nanoparticles with PAA shell thicknesses of 5, 16, and 32 nm, respectively.

flat films after MSAT, which show tan-yellow and yellowish-green color, respectively (Figure 3e II and III). The two colors originate from the high refractive index of CdS, coherent scattering of natural light by CdS@PAA nanoparticles, and intrinsic cadmium yellow, rather than the structural colors of PCs. In stark contrast, the CdS@PAA(32 nm shell)-AA slurry could form a smooth PC film with uniform and ultra-bright green structural color after MSAT (Figure 3e IV), which completely suppresses the intrinsic cadmium yellow of nanoparticles. The reflection spectra of the sheet-like CdS-AA mixture and the three films are illustrated in Figure 3f. No reflection signal from the sheet-like CdS-AA mixture is observed. The films fabricated from CdS@PAA (5 nm shell)-AA and the CdS@PAA (16 nm shell)-AA slurries also show negligible reflection signals. Oppositely, the film fabricated from the CdS@PAA (32 nm shell)-AA slurry displays a sharp reflection peak located at 513 nm, which is in good agreement with its green structural color. The reflection intensity is up to 143%, proving the strong PBG and the high structural color saturation of the ultra-bright PC film.

The above distinctions can be explained by the fact that AA molecules adequately swell and soften the thick PAA shells, inducing the CdS@PAA (32 nm shell)-AA slurry to generate higher viscosities than the CdS@PAA (5 nm shell)-AA and the CdS@PAA (16 nm shell)-AA slurries. The shearing force can be effectively delivered to per CdS@PAA (32 nm shell) nanoparticle during MSAT, stimulating stronger interactions between CdS@PAA (32 nm shell) nanoparticles than that of the CdS@PAA (5 nm shell) and the CdS@PAA (16 nm shell) nanoparticles under shear. The enhanced interparticle interactions are competent to effectively drive all CdS@PAA (32 nm shell) nanoparticles to assemble into long-range ordered photonic structure (Figure 3j). However, the weak interparticle interactions of the CdS@PAA(16 nm shell) or CdS@PAA (5 nm shell) nanoparticles merely drive corresponding nanoparticles to arrange into short-range ordered or disordered structures (Figure 3i,h). As a result, the CdS@PAA (32 nm shell)-AA slurry can generate the ultra-bright PC film with a highly ordered structure after MSAT. Besides, the process from CdS@PAA(32 nm shell)-AA slurry to the ultra-bright PC

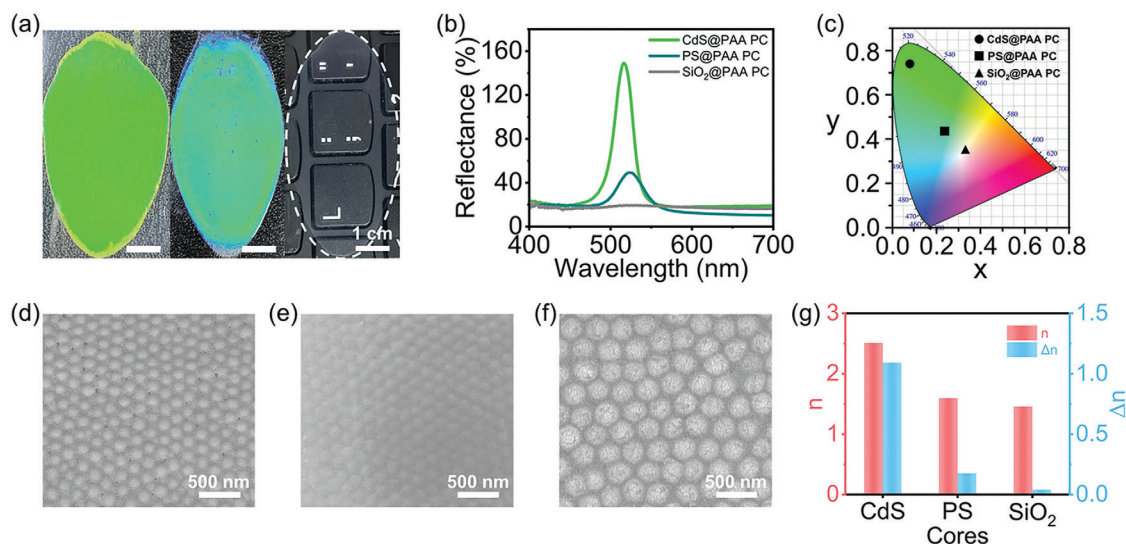


**Figure 4.** Performance comparison between the as-prepared ultra-bright PC film and conventional PC films. a) Digital photographs of the PC films constructed by various assembling blocks: CdS@PAA, PS@PAA, and SiO<sub>2</sub>@PAA nanoparticles (from left to right). b) Corresponding reflection spectra and c) CIE chromaticity diagram of the three PC films. SEM images of the PC films constructed from d) CdS@PAA, e) PS@PAA, and f) SiO<sub>2</sub>@PAA nanoparticles, respectively. g) Refractive indices  $n$  of different cores in various assembling blocks as well as refractive index contrasts ( $\Delta n$ ) between these cores and AA matrix, respectively.

film requires only MSAT of one or two times (Figure S10, Supporting Information). The optical properties of the ultra-bright PC film remain constant under incremental MSAT times. Therefore, in other words, a necessary condition for preparing the ultra-bright PC film through the MSAT is to endow the assembly block CdS@PAA nanoparticles with suitable PAA shell thickness.

#### 2.4. Excellent Optical Performances of the Ultra-Bright PC Film

The ultra-bright PC film exhibits higher structural color saturation and stronger PBG than conventional PC films. Conventional PC films are commonly fabricated with polystyrene (PS) microspheres or SiO<sub>2</sub> nanoparticles as assembly units. Here, CdS@PAA, PS@PAA, and SiO<sub>2</sub>@PAA nanoparticles with similar PAA shell thickness were synthesized (Figure S11, Supporting Information). The different cores including CdS, PS, and SiO<sub>2</sub> possess different refractive indices. After the corresponding slurries containing the same mediator molecule AA were subjected to the MSAT, the CdS@PAA, PS@PAA, and SiO<sub>2</sub>@PAA nanoparticles as assembly blocks were assembled into PC films, respectively. As illustrated in Figure 4a, the CdS@PAA PC and the PS@PAA PC films show ultra-bright green and plain green structural colors, respectively. However, the SiO<sub>2</sub>@PAA PC film is transparent. The corresponding reflection spectra of three PC films are shown in Figure 4b. The reflection signals of the three PC films appear around the wavelength of 517 nm. The relative reflection intensity of the CdS@PAA PC film is as high as 130%, exceeding four times PS@PAA PC film (30%). The relative reflection intensity is defined here as the difference between the highest point of reflection peak and the baseline of reflection spectra. In addition, the reflection spectrum of the SiO<sub>2</sub>@PAA PC film has no reflection signal. Even after expanding the detection wavelength range from 400–700 to 400–1100 nm, no significant

reflection peak appears in the spectrum (Figure S12, Supporting Information). Thereby the reflection intensity of the SiO<sub>2</sub>@PAA PC film can be neglected. This distinction in reflection intensities demonstrates that the CdS@PAA PC film possesses a brighter structural color and stronger PBG than the PS@PAA PC and SiO<sub>2</sub>@PAA PC films. Among them, the PBG of the SiO<sub>2</sub>@PAA PC film is the weakest. Therefore, the CdS@PAA PC film starkly reflects the green light and the PS@PAA PC film to a lesser extent, while the SiO<sub>2</sub>@PAA PC film with high transparency barely reflects lights. The CIE diagram indicates that the CIE coordinates of the SiO<sub>2</sub>@PAA PC, PS@PAA PC, and CdS@PAA PC film are consistent with their structural colors, and present a trend from center to edge (Figure 4c). The CIE coordinate of the CdS@PAA PC film is located at the very edge of the CIE diagram, confirming the high structural color saturation of the CdS@PAA PC film.

The difference among the CdS@PAA PC, PS@PAA PC, and SiO<sub>2</sub>@PAA PC films in reflection intensity and structural color saturation can be attributed to the difference in the refractive index contrast ( $\Delta n$ ) between the components that make up these PC films. Here, the components of these PC films are different assembly blocks and the same mediator molecule. In this section, considering the PAA shells of the three assembly blocks are consistent, we only calculate the  $\Delta n$  between various cores and mediator molecule AA in the ideal state. Under the premise of PC films with highly ordered periodic structures (Figure 4d–f), the  $\Delta n$  is positively correlated with the reflection intensity of the PC films. The  $\Delta n$  mainly comes from the contrasts between the refractive indices of CdS, PS, and SiO<sub>2</sub> and PAA. The refractive index of CdS is 2.51, which is much greater than 1.595 for PS and 1.4585 for SiO<sub>2</sub> (Figure 4g). The refractive index of PAA is 1.4185. Therefore, the  $\Delta n$  in CdS@PAA PC, PS@PAA PC, and SiO<sub>2</sub>@PAA PC films are determined to be 1.0915, 0.1765, and 0.04, respectively (Figure 4g). The large  $\Delta n$  endows PC films with

high reflection intensity (Figure S13, Supporting Information). The above data sufficiently proved that the CdS@PAA PC film possesses a brighter structural color and higher reflection intensity than conventional PC films.

## 2.5. Manipulation of Reflection Intensity of PC Films

The reflection intensity of the ultra-bright PC film can also be well manipulated by controlling the cross-linking degree of the PAA shells of the CdS@PAA nanoparticles. Here, nine batches of CdS@PAA composite nanoparticles with the incremental cross-linking degrees of the PAA shells from 0% to 28.6% were synthesized (Figures S14 and S15, Supporting Information). The particle size of CdS cores and the thickness of PAA shells were fixed at  $\approx 115$  and 32 nm, respectively. When the cross-linking degree is 0%, the CdS@PAA nanoparticles have no clear core-shell structure and the CdS nanoparticles are promiscuously distributed in the PAA matrix. With the cross-linking degrees of PAA shells increasing from 4.8% to 28.6%, the CdS@PAA nanoparticles keep clear core-shell structures. After these CdS@PAA nanoparticles with different PAA cross-linking degrees were subjected to MSAT, except for the rough CdS@PAA film with PAA cross-linking degree of 0% shows intrinsic cadmium yellow without reflection signal, the other obtained smooth CdS@PAA PC films display green structural colors (Figure 5a). Interestingly, the brightness of structural colors and reflection intensities of these PC films gradually increase as PAA cross-linking degrees increase from 4.8% to 25.9% (Figure 5b). Finally, the CdS@PAA PC film with a PAA cross-linking degree of 28.6% re-displays dim green structural color and weak reflection intensity, the corresponding CIE diagram is illustrated in Figure 5c. The CIE coordinates of the nine films with different PAA cross-linking degrees follow a trend from the center to the edge and finally back to the center as the PAA cross-linking degrees elevate from 0% to 28.6%, indicating the color saturation of PC film change process.

The regular variation of reflection intensities of PC films with the PAA cross-linking degrees is unique and obvious (Figure 5d). Different refractive index contrast ( $\Delta n$ ) in these PC films is the main reason for the regular variation. Considering the PAA shells with different cross-linking degrees cause differences in the refractive indices of CdS@PAA nanoparticles, we define that the  $\Delta n$  in these PC films mainly derives from the contrasts between assembly block CdS@PAA nanoparticles and mediator molecule AA in refractive indices. Here, the refractive index of the AA, the cross-linker DVB, and the CdS are determined to be 1.4185, 1.561, and 2.51, respectively. The refractive index of PAA with different cross-linking degrees and corresponding CdS@PAA can be calculated by Equations (3) and (4), respectively.

$$n_{\text{PAA}} = (n_{\text{AA}}^2 f_{\text{AA}} + n_{\text{DVB}}^2 f_{\text{DVB}})^{1/2} \quad (3)$$

$$n_{\text{CdS@PAA}} = (n_{\text{CdS}}^2 f_{\text{CdS}} + n_{\text{PAA}}^2 f_{\text{PAA}})^{1/2} \quad (4)$$

where,  $n_{\text{PAA}}$ ,  $n_{\text{AA}}$ , and  $n_{\text{DVB}}$  represent the refractive indices of the PAA, AA, and DVB, respectively;  $f_{\text{AA}}$  and  $f_{\text{DVB}}$  are the volume fractions of the AA and DVB, respectively;  $n_{\text{CdS@PAA}}$  and  $n_{\text{CdS}}$  represent the refractive indices of the CdS@PAA and CdS, respec-

tively;  $f_{\text{CdS}}$  and  $f_{\text{PAA}}$  are the volume fractions of CdS and PAA, respectively.

The calculated refractive indices of PAA and corresponding CdS@PAA enlarge gradually as the cross-linking degrees of the PAA enhance from 0% to 28.6% (Figure 5e). The  $\Delta n$  in different PC films also accordingly increase due to the identical refractive index of the mediator molecule AA (Figure 5f). In the context of the long-range ordered structures of PC films, the large  $\Delta n$  gives rise to a high reflection intensity and improved structural color brightness.

The microstructures of the PC films with various cross-linking degrees of PAA shells were characterized, as illustrated in Figure 5g–o. When the cross-linking degree of PAA is 0%, the CdS nanoparticles messily distribute in a mass PAA matrix (Figure 5g), which explains the intrinsic cadmium yellow of the rough CdS@PAA film. The small  $\Delta n$  and limited long-range ordered structures synergistically render that the PC film with a PAA cross-linking degree of 4.8% presents a low reflection intensity and poor structural color saturation (Figure 5h). When the cross-linking degrees of PAA are in the range of 9.1–25.9%, all PC films possess long-range ordered structures (Figure 5i–n), indicating the optical properties of these PC films are governed by the corresponding  $\Delta n$ . Under the PAA cross-linking degree of 28.6%, a large  $\Delta n$  corresponds instead to a poor structural color saturation and weak reflection intensity, which can be explained by the short-range ordered structure of the PC film (Figure 5o). Increasing the cross-linking degree of PAA not only enlarges the  $\Delta n$  in PC films, but also facilitates the protection of the core-shell structure of composite nanoparticles during the MSAT, promotes effective transfer of the shearing force and assembly of CdS@PAA nanoparticles into the long-range ordered structure, finally realizes the ultra-bright PC films. Nevertheless, when the cross-linking degree of PAA exceeds a certain critical value, the mediator molecule AA cannot swell and soften the PAA shell, weakening the interparticle interaction of the assembly block CdS@PAA nanoparticles, resulting in short-range ordered or disordered structures, ultimately obtaining PC films with poor optical properties. Therefore, adjusting the cross-linking degree of PAA shells is an effective strategy for achieving the manipulation of structural colors and reflection intensity of the PC films.

## 2.6. Control of the PC Structural Colors

The structural colors of the ultra-bright PC films can be controlled by changing the particle size of assembly unit CdS nanoparticles. Here, six groups of CdS nanoparticles with particle sizes of 92, 115, 126, 135, 147, and 170 nm were encapsulated with PAA shell and assembled into the ultra-bright PC films through MSAT, respectively. These obtained ultra-bright PC films show vibrant blue, green, yellow, red, crimson, and infrared structural colors, respectively (Figure 6a). The various structural colors of these ultra-bright PC films cover the entire visible area and display high structural color saturation (Figure 6b). The corresponding reflection spectra are illustrated in Figure 6c. The reflection wavelengths of the different ultra-bright PC films are located at 470, 520, 588, 618, 659, and 732 nm, respectively, in good agreement with their structural colors. When the particle

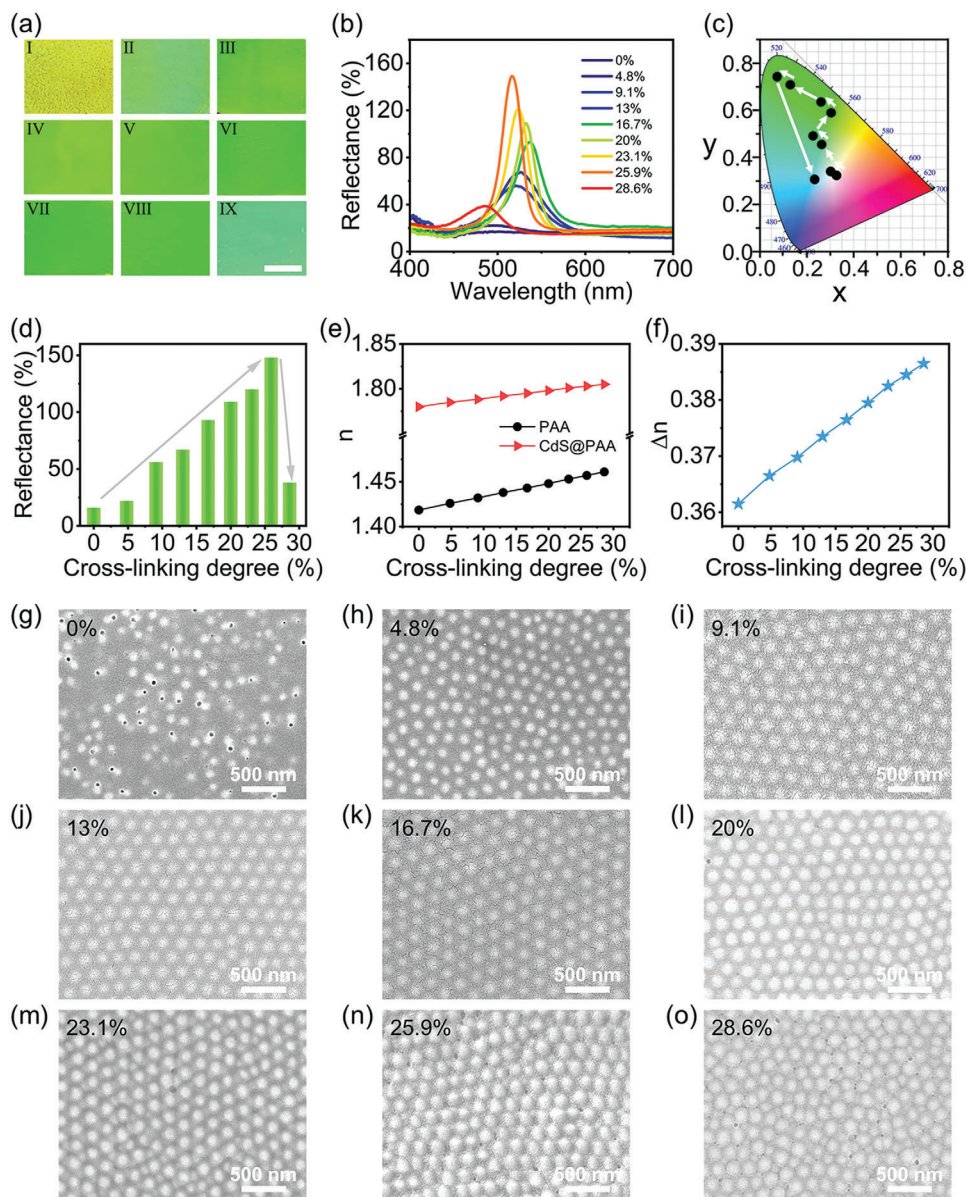


**Figure 5.** Regulation of reflection intensity of the PC films. a) Digital photographs of PC films constructed by CdS@PAA nanoparticles with different cross-linking degrees of PAA shells: (I) 0%, (II) 4.8%, (III) 9.1%, (IV) 13%, (V) 16.7%, (VI) 20%, (VII) 23.1%, (VIII) 25.9%, and (IX) 28.6%. The scale bar is 1 cm. b) Corresponding reflection spectra and c) CIE chromaticity diagram of the nine PC films. d) Relationship between reflection intensity of PC films and cross-linking degree of PAA shells. e) Refractive indices ( $n$ ) of PAA and CdS@PAA as a function of the cross-linking degree of PAA shell, respectively. f) Refractive index contrast ( $\Delta n$ ) in PC films as a function of the cross-linking degree of PAA shell. g–o) SEM images of PC films with different cross-linking degrees of PAA.

size increases to 147 and 170 nm, the structural colors of the as-prepared photonic crystal films redshift to the near-infrared region, resulting in the weak and invisibility of the structural color of photonic crystals, and the intrinsic cadmium yellow color of CdS nanoparticles is visible. Thus, the macroscopic color of the photonic crystal film appears yellow.

All reflection peaks in Figure 6c are slender, indicating that the PC films with various structural colors possess high reflection intensities and strong PBGs. The normalized full width at half-maximum (FWHM) is defined as the ratio of the peak width at half the height of the reflection

wavelength.<sup>[34]</sup> The normalized FWHM of the ultra-bright PC films with various structural colors are all less than 0.1, implying the superior quality in the photonic structure of these ultra-bright PC films (Figure 6d). Ten positions were taken on each PC film to measure the reflection signal, and there were only negligible fluctuations in the reflection wavelength among the ten positions (Figure 6e). The stability of the reflected wavelength reflects the uniformity of the optical properties of ultra-bright PC films in the case of large film area. Finally, SEM images directly reveal the highly ordered structures of these ultra-bright PC films with various structural colors (Figure 6f–k). This result corresponds well

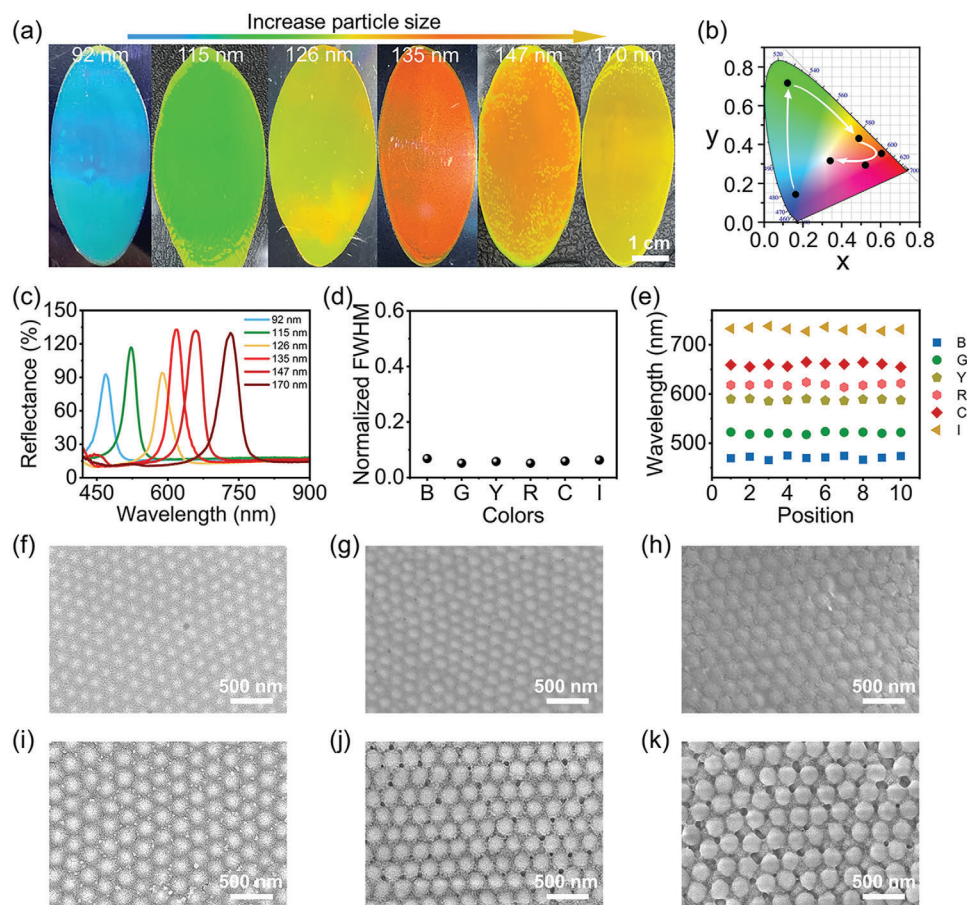


**Figure 6.** Structural color regulation of the ultra-bright PC films. a) Digital photographs of the ultra-bright PC films with different structural colors fabricated by increasing particle sizes of CdS cores from 92 to 115, 126, 135, 147, and 170 nm. b) Corresponding CIE chromaticity diagram and c) reflection spectra. d) Normalized FWHM of the ultra-bright PC films with different structural colors. e) Reflection wavelength of random 10 positions on the ultra-bright PC films with different structural colors. B, G, Y, R, C, and I represent blue, green, yellow, red, crimson, and infrared structural colors, respectively. SEM images of the ultra-bright PC films with different structural colors constructed from CdS nanoparticles with particle sizes of f) 92, g) 115, h) 126, i) 135, j) 147, and k) 170 nm.

to the excellent optical properties of these ultra-bright PC films. The multi-selection in structural colors will greatly enhance the application value of the ultra-bright PC films.

## 2.7. Display for Anticounterfeiting Coatings

The ultra-bright PC films can be applied in many fields, such as for anticounterfeiting coatings. As a demonstration, the PC paint was fabricated by embedding the stimuli-responsive ultra-bright PC pigments within a transparent matrix. The fabrication process is shown in **Figure 7a**. The selected ultra-bright PC films were prepared by CdS@PAA nanoparticles with CdS core sizes of 115 (green), 126 (yellow), and 135 (red) nm. The ultra-bright PC film was firstly mashed into small PC fragments as pigment, and then the PC pigment was blended with PDMS and stirred to mix them evenly, the PC paint was finally prepared. Due to the high reflection intensity of the PC pigment, the PC paint shows bright structural colors (**Figure 7b**). This result also suggests that the periodically ordered structure of the ultra-bright PC film is solid and undamaged after mashing. The PC paint had an ideal

leveling property and could be coated on a flat substrate. After hot-curing, smooth PC coating formed (**Figure 7c**). The obtained PC coating exhibits vivid structural colors with a uniform color distribution. Moreover, the PC paint is also capable of being applied on three-dimensional substrates. For example, after coating the PC paint on a car model, the car model shows a shiny and brilliant appearance (**Figure 7d**), which means that the PC paints display a widespread application range including decoration and automotive coatings.

The as-prepared PC coating exhibited excellent mechanical stability. Herein, a green PC coating was selected for durability tests (**Figure 7e**). The PC coating was bent back and forth 100 times, rubbed 100 times using sandpaper, and brushed 100 times using a test-tube brush, respectively (**Figure 7f–h**). After all these tests were finished, the appearance of the PC coating remained consistent with its original state. This result indicates that the PC coating has reliable resistance under violent mechanical actions. Thus, the as-prepared PC coatings meet the requirements of various environments for practical use.

The PC coating also can achieve a stimuli-responsive effect that responds to water. According to our previous report,<sup>[35]</sup>

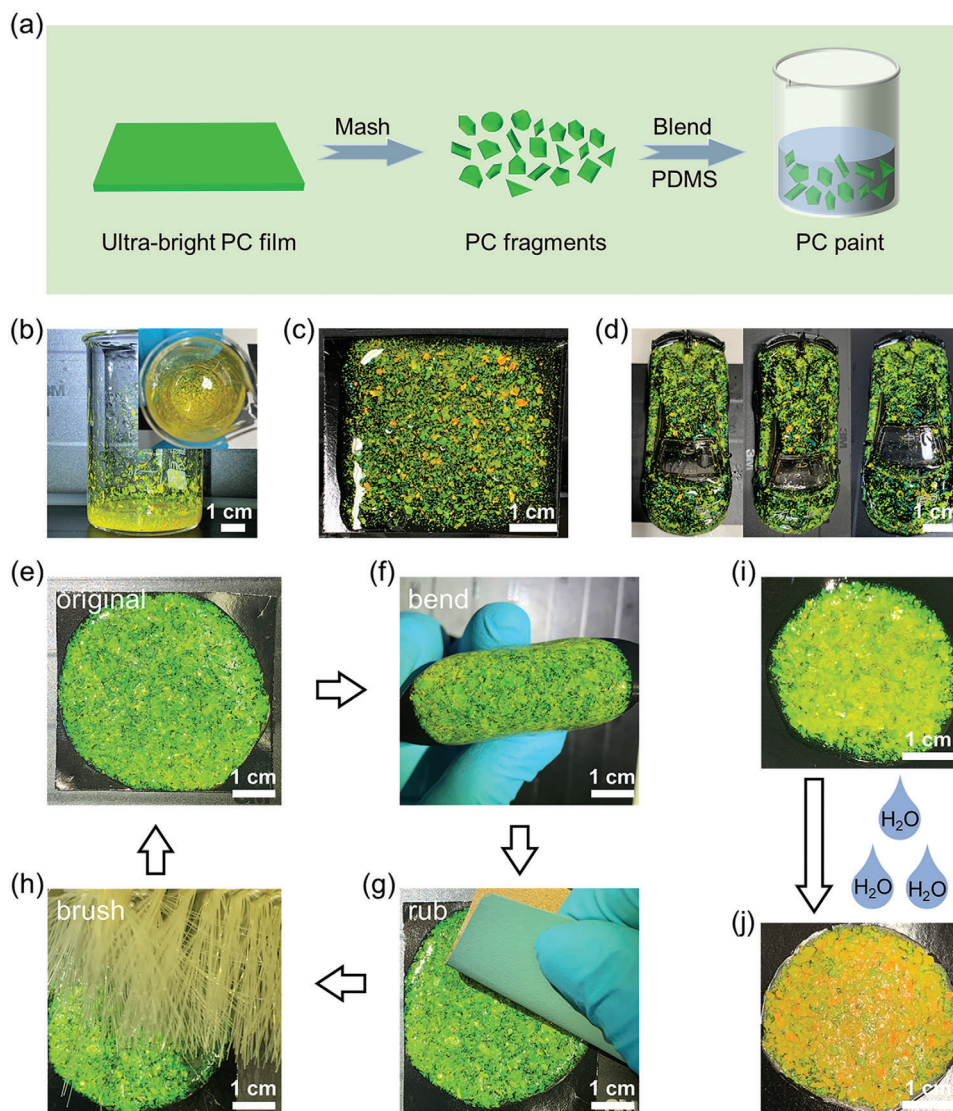


**Figure 7.** Fabrication and application of water stimuli-responsive anticounterfeiting PC coating. a) Schematic illustration of fabricating the PC paint. b) Digital photographs of PC paint. The inset is a top view. c,d) Digital photographs of the PC coating on (c) a flat substrate and (d) a car model, respectively. e–h) Digital photographs of (e) original PC coating and the sample after being (f) bent, (g) rubbed, and (h) brushed 100 times, respectively. i,j) Digital photographs of the anticounterfeiting PC coating in (i) dry and (j) contacted with water, respectively.

before mashing, sodium hydroxide solution ( $\text{pH} = 13$ ) was used to introduce hygroscopic salt in a green ultra-bright PC film. After drying, the PC film exhibited high hydrophilicity due to the transformation from PAA to polyacrylic acid sodium salt (PAAS). The hydrophilicity can be maintained during the fabrication of the smart PC coating. To achieve water response PC coatings, the pigment volume concentration (PVC) of the PC paint must be greater than its critical pigment volume concentration (CPVC). In the dry state, the smart PC coating showed a vivid green color (Figure 7i). Once in contact with water, the water infiltrated the PC coating, the color of the PC pigment redshifted, and the PC coating switched to yellow-red colors (Figure 7j). This is because the hydrophilic PAAS matrix absorbs water in the PC coating and swells, causing an increase in interparticle spacing between the CdS cores. The PC coating that responds to water can intuitively

monitor whether the coated facilities is in contact with water. Meanwhile, it possesses a high level of anticounterfeit property, water can be used as the probe.

### 3. Conclusion

In summary, a new kind of ultra-bright PC film was prepared by assembling CdS@PAA core-shell nanoparticles through scalable molecule-mediated shearing-induced assembly technique (MSAT) under room temperature, the high refractive index of CdS is the basis for the high brightness of PC film. Due to the highly ordered structures of the PC films, the ultra-bright structural colors can suppress intrinsic cadmium yellow, thus the PC films show a stable iridescence effect. This work also demonstrated that the slurry with appropriate viscosity and

enhanced interparticle interaction between CdS@PAA nanoparticles is the key condition for preparation of the ultra-bright PC film using MSAT, and the related condition can be achieved by regulating the thickness of the PAA shell. Compared with conventional PCs prepared with PS or SiO<sub>2</sub> core nanoparticles, this new kind of ultra-bright PC film exhibits stronger reflection intensity and higher structural color saturation due to the larger refractive index contrast. As required for use, the reflection intensity of the ultra-bright PC films can be precisely manipulated by controlling the cross-linking degree of the PAA shell. The ultra-bright PC films with various structural colors can be obtained by changing the CdS core particle size. These ultra-bright PC films with different structural colors have excellent optical performances, their reflection wavelengths cover the entire visible region. Besides, the PC paint was prepared by mashing the ultra-bright PC film and blending it with transparent PDMS matrix. In addition, the PC coating prepared by alkali treated ultra-bright PC pigments can achieve water response effect and anticounterfeit ability. This work not only provides a new strategy for assembling inorganic nanoparticles with high refractive index into PCs, but also boosts the improvement in the quality of PCs. Eventually, the ultra-bright PC films exhibit great application potential in the fields of automotive coatings, anticounterfeiting, colorful displays, and optical devices.

#### 4. Experimental Section

**Materials:** Polyvinylpyrrolidone (PVP,  $M_w$ :40 000, K40) was purchased from Sigma-Aldrich. Diethylene glycol (DEG, 99%), thiourea (TU, 99%), cadmium nitrate tetrahydrate (Cd(NO<sub>3</sub>)<sub>2</sub>·4H<sub>2</sub>O, 99.99%), acrylic acid (AA, 99%), divinylbenzene (DVB, 80%), 2,2'-azobis(2-methylpropionitrile) (AIBN, 99%), and benzoyl peroxide (BPO, 99%) were purchased from Shanghai Aladdin Chemistry Co. Ltd. (China). Acetonitrile (99%) and ethanol (95%) were purchased from Sinopharm Chemical Reagent Co., Ltd. (China). Polydimethylsiloxane (PDMS, Sylgard 184) was purchased from Dow Corning. All chemicals were used as received without further purification.

**Synthesis of Monodisperse CdS Nanoparticles:** Monodisperse CdS nanoparticles with adjustable particle size can be synthesized through a high-temperature synthesis reaction. Typically, 5 g PVP was first mixed into 150 mL DEG in a 250 mL beaker. Then, the mixture was stirred at 600 rpm until the PVP was completely dissolved at room temperature. The obtained transparent solution was transferred into a 250 mL three-necked flask and connected heat-stir device. The transparent solution was heated to 80 °C for 30 min accompanied by the stir. Subsequently, TU (0.988 g) and Cd(NO<sub>3</sub>)<sub>2</sub>·4H<sub>2</sub>O (4.004 g) were separately mixed into the transparent solution under 80 °C. After the TU and Cd(NO<sub>3</sub>)<sub>2</sub>·4H<sub>2</sub>O were completely dissolved, the temperature of the mixture system was gradually raised to 160 °C. After the reaction was sustained for 1 h at 160 °C. The transparent solution turns into a yellow suspension. Next, the heat was removed and the yellow suspension was naturally cooled to room temperature. The stir was continuous throughout the whole reaction and cooling process. Then, the yellow suspension was poured into 300 mL ethanol in an 800 mL beaker and stirred well. The monodisperse CdS nanoparticles with a particle size of 170 nm were collected by centrifuging (12 000 rpm, 10 min) the obtained yellow suspension. Finally, the collected CdS nanoparticles were washed five times with excessive ethanol through alternate centrifugation and sonication. According to the same process, the CdS nanoparticles with different particle sizes were synthesized by altering the amounts of TU and Cd(NO<sub>3</sub>)<sub>2</sub>·4H<sub>2</sub>O under their molar ratio kept at 1:1. All collected monodisperse CdS nanoparticles with various particle sizes were dispersed in ethanol for further use.

**Synthesis of Composite CdS@PAA Core-Shell Nanoparticles:** The composite CdS@PAA core-shell nanoparticles were synthesized through one-step reflux precipitation polymerization (ORPP) reaction. In this reaction, AA is the monomer, DVB is the cross-linker, and AIBN is the initiator. Typically, 100 mg CdS nanoparticles were uniformly dispersed in 120 mL acetonitrile in a 250 mL single-necked flask. Afterward, 1 g PVP was added into the dispersion with a stir for 30 min and sonicated for 10 min. Subsequently, 500 μL AA, 175 μL DVB, and 25 mg AIBN were added to the dispersion. After 10 min of sonication, the homogeneous dispersion was heated to 110 °C within 10 min and maintained in its boiling state for 3 h with a stir. Then, the heat was ceased and the polymerization reaction system was naturally cooled to room temperature. The composite CdS@PAA core-shell nanoparticles with a PAA shell thickness of 32 nm were collected by centrifuging (12 000 rpm, 8 min) the final dispersion. The thicknesses of the PAA shells can be changed by altering the amounts of AA monomer. The collected CdS@PAA core-shell nanoparticles were washed five times with excessive ethanol through alternate centrifugation and sonication. Finally, the composite CdS@PAA core-shell nanoparticles were freeze-dried for 48 h using a freeze dryer (SCIENTZ-10N, Ningbo Xinzhi Biotechnology Co., Ltd.) for further use.

**Preparation of Ultra-Bright PC Films:** The ultra-bright PC films were prepared through a high-throughput technique called the molecule-mediated shearing-induced assembly technique (MSAT) at room temperature. Typically, the mediator molecule solution was first prepared by homogeneously mixing 1 mL AA (mediator molecules), 200 μL DVB (cross-linker), and 30 mg BPO (thermal curing agent) under oscillation and sonication. Then, the 50 μL mediator molecule solution was blended with 50 mg CdS@PAA core-shell nanoparticles under stir to form a viscous CdS@PAA-AA slurry. The volume fraction of the CdS@PAA core-shell nanoparticles in the viscous CdS@PAA-AA slurry is 33.3%. Subsequently, 30 mg slurry was tightly sandwiched between two pieces of poly(ethylene terephthalate) (PET) films under gentle pressure with hands to form a PET-slurry-PET sandwiched structure. The formed PET-slurry-PET films were then inserted into the gap between the two rollers rotating inward in the MSAT machine. At room temperature, the MSAT machine was activated to squeeze and bend the slurry rotationally. The CdS@PAA core-shell nanoparticles were subjected to sufficient shearing forces and assembled into highly ordered arrays. After several MSAT processes, the ultra-bright PC films with high structural color saturation were obtained. Finally, the ultra-bright PC films were placed in a blast oven with a preheated temperature of 90 °C and heated for 12 h to solidify their photonic structures.

**Fabrication of PC Paint:** The PC paint can be fabricated by combining the ultra-bright PC pigments and a transparent matrix. The transparent matrix is PDMS containing 9 wt% Sylgard 184 elastomer kit (cross-linker). Typically, the ultra-bright PC films were first mashed into PC pigments using an agate mortar. Then, these obtained PC pigments were mixed with the transparent matrix with a mass ratio of 1:4. After the mixture was stirred well, the PC paint formed. Subsequently, the PC paint was uniformly coated on substrates and cured in a blast oven with a preheated temperature of 70 °C for 2.5 h. Finally, the shiny and vivid PC coating was successfully fabricated.

**Characterization:** The scanning electron microscope (SEM) images were collected by the Cryo-FESEM, Zeiss Gemini SEM500 at an operating voltage of 3 kV and a working distance of 5.0–8.0 mm. The transmission electron microscope (TEM) images were captured using the HCTEM, HITACHI HT7800 at an accelerating voltage of 100 kV. The particle size distribution of nanoparticles was measured using Nano Measurer (China) software. The optical microscope image was obtained on the Polarizing Microscope, Leica DM2500P. The 2D ultra-small angle X-ray scattering (USAXS) patterns were obtained at Beamline BL10U1 from the Shanghai Synchrotron Radiation Facility (SSRF) in China. The X-ray wavelength used was 0.124 nm. The USAXS detector employed was an Eiger 4 M, with the detector positioned 27 600 mm away from the sample and a pixel size of 75 μm. The number of pixels on the x and y axes were 2070 and 2167, respectively. The exposure time was set to 20 s, and the obtained USAXS data was analyzed using FIT 2D software. The reflection spectra were measured using a Choptics EK2000-Pro spectrometer with an IdeoOptics FIB-Y-600-UV fiber and a Choptics LS2000-DH light source. A standard

aluminum mirror was used as the reference and its reflectance was defined as 100%. The CIE chromaticity diagram was converted from the reflection spectra. The angle-resolved reflection spectra were recorded using an angle-resolved spectrum instrument (R1, Ideaoptics, China) equipped with a highly sensitive spectrometer (NOVA, Ideaoptics, China). The X-ray diffraction (XRD) patterns were obtained using an X-ray Diffractometer, Rigaku SmartLab 9KW. The rheology measurements including storage modulus ( $G'$ ), loss modulus ( $G''$ ), and viscosity ( $\eta$ ) were implemented on a Modular Rheometer Platform (Haake MARS III, Thermofisher). All digital photographs were taken with a smartphone (iPhone XR).

## Supporting Information

Supporting Information is available from the Wiley Online Library or from the author.

## Acknowledgements

The authors thank the financial support from the National Natural Science Foundation of China (Grant Nos. 52131308, 52373131), MOST (2022YFA1203002).

## Conflict of Interest

The authors declare no conflict of interest.

## Data Availability Statement

The data that support the findings of this study are available from the corresponding author upon reasonable request.

## Keywords

anticounterfeiting, assembly technique, photonic crystals, smart coatings, structural color

Received: October 14, 2024  
Revised: November 16, 2024  
Published online: December 9, 2024

- [1] a) M. Sakai, T. Seki, Y. Takeoka, *Small* **2018**, *14*, 1800817; b) H. Huang, H. Li, X. Shen, K. Gu, J. Guo, C. Wang, *Chem. Eng. J.* **2022**, *429*, 132437.
- [2] a) L. Li, Z. Yu, C. Ye, Y. Song, *Adv. Funct. Mater.* **2024**, *34*, 2311845; b) X. Hou, F. Li, Y. Song, M. Li, *J. Phys. Chem. Lett.* **2022**, *13*, 2885.
- [3] Q. Fu, W. Yu, G. Bao, J. Ge, *Nat. Commun.* **2022**, *13*, 7007.
- [4] W. Hong, Z. Yuan, X. Chen, *Small* **2020**, *16*, 1907626.
- [5] H. Li, G. Zhao, M. Zhu, J. Guo, C. Wang, *ACS Appl. Mater. Interfaces* **2022**, *14*, 14618.
- [6] Y. Li, Q. Fan, X. Wang, G. Liu, L. Chai, L. Zhou, J. Shao, Y. Yin, *Adv. Funct. Mater.* **2021**, *31*, 2010746.
- [7] X. Li, X. Wang, Y. Wang, M. Hu, G. Liu, L. Chai, L. Zhou, J. Shao, Y. Li, *Small* **2024**, *20*, 2302550.
- [8] a) M. Kuang, J. Wang, L. Jiang, *Chem. Soc. Rev.* **2016**, *45*, 6833; b) A. G. Dumanli, T. Savin, *Chem. Soc. Rev.* **2016**, *45*, 6698.
- [9] a) R. Xiong, J. Luan, S. Kang, C. Ye, S. Singamaneni, V. V. Tsukruk, *Chem. Soc. Rev.* **2020**, *49*, 983; b) Z. Cai, Z. Li, S. Ravaine, M. He, Y. Song, Y. Yin, H. Zheng, J. Teng, A. Zhang, *Chem. Soc. Rev.* **2021**, *50*, 5898; c) Z. Li, Y. Yin, *Adv. Mater.* **2019**, *31*, 1807061.
- [10] a) J. F. Galisteo-López, M. Ibisate, R. Sapienza, L. S. Froufe-Pérez, Á. Blanco, C. López, *Adv. Mater.* **2011**, *23*, 30; b) C. I. Aguirre, E. Reguera, A. Stein, *Adv. Funct. Mater.* **2010**, *20*, 2565.
- [11] a) S. Wu, H. Xia, J. Xu, X. Sun, X. Liu, *Adv. Mater.* **2018**, *30*, 1803362; b) G.-X. Li, T. Dong, L. Zhu, T. Cui, S. Chen, *Chem. Eng. J.* **2023**, *453*, 139763.
- [12] W. Zhang, Y. Hu, P. Feng, Z. Li, H. Zhang, B. Zhang, D. Xu, J. Qi, H. Wang, L. Xu, Z. Li, M. Xia, J. Li, R. Chai, L. Tian, *Adv. Sci.* **2024**, *11*, 2403173.
- [13] J. Liao, C. Ye, P. Agrawal, Z. Gu, Y. S. Zhang, *Small Struct.* **2021**, *2*, 2000110.
- [14] E. S. A. Goerlitzer, R. N. Klupp Taylor, N. Vogel, *Adv. Mater.* **2018**, *30*, 1706654.
- [15] a) J. He, X. Shen, H. Li, Y. Yao, J. Guo, C. Wang, *ACS Appl. Mater. Interfaces* **2022**, *14*, 27251; b) H. Huang, J. Yin, Q. Zhou, H. Li, J. Yang, Y. Wang, M. Xu, C. Wang, *Nat. Commun.* **2024**, *15*, 3999.
- [16] a) H. Li, M. Zhu, F. Tian, W. Hua, J. Guo, C. Wang, *Chem. Eng. J.* **2021**, *426*, 130683; b) H. Huang, H. Li, J. Yin, K. Gu, J. Guo, C. Wang, *Adv. Mater.* **2023**, *35*, 2211117.
- [17] a) T. Li, G. Liu, H. Kong, G. Yang, G. Wei, X. Zhou, *Coord. Chem. Rev.* **2023**, *475*, 214909; b) X. Dong, P. Wu, C. G. Schaefer, L. Zhang, C. E. Finlayson, C. Wang, *Mater. Des.* **2018**, *160*, 417; c) G. H. Lee, T. M. Choi, B. Kim, S. H. Han, J. M. Lee, S.-H. Kim, *ACS Nano* **2017**, *11*, 11350.
- [18] a) Y. Fang, H. Li, X. Wang, M. Zhu, J. Guo, C. Wang, *ACS Appl. Nano Mater.* **2022**, *5*, 11249; b) Q. Guo, J. Guo, C. Wang, *Adv. Optical Mater.* **2024**, *12*, 2401139.
- [19] a) L. Feng, S. Natu, V. Som de Cerff Edmonds, J. J. Valenza, *Nat. Commun.* **2022**, *13*, 567; b) X. Shen, P. Wu, C. G. Schäfer, J. Guo, C. Wang, *Nanoscale* **2019**, *11*, 1253.
- [20] a) Q. Guo, X. Wang, J. Guo, C. Wang, *Nanoscale* **2023**, *15*, 18825; b) X. Zhang, T. Yin, J. Ge, *Adv. Mater.* **2024**, *36*, 2309344.
- [21] M. Zhu, H. Li, Q. Guo, J. Guo, C. Wang, *ACS Appl. Mater. Interfaces* **2024**, *16*, 32543.
- [22] a) Y. Xie, Y. Meng, W. Wang, E. Zhang, J. Leng, Q. Pei, *Adv. Funct. Mater.* **2018**, *28*, 1802430; b) Z. Wang, S. Zhang, B. Tang, *ACS Nano* **2024**, *18*, 186.
- [23] a) Y. Fang, W. Fei, X. Shen, J. Guo, C. Wang, *Mater. Horiz.* **2021**, *8*, 2079; b) Y. Ji, W. Xu, I. L. Rasskazov, H. Liu, J. Hu, M. Liu, D. Zhou, X. Bai, H. Ågren, H. Song, *Appl. Phys. Rev.* **2022**, *9*, 041319.
- [24] Y.-H. Ra, C.-R. Lee, *Nano Energy* **2021**, *84*, 105870.
- [25] a) W. Wei, C. Wu, Q. Fang, Z. Zhao, X. Su, *J. Mater. Chem. C* **2023**, *11*, 12667; b) M. G. Han, C. G. Shin, S. J. Jeon, H. Shim, C. J. Heo, H. Jin, J. W. Kim, S. Lee, *Adv. Mater.* **2012**, *24*, 6438; c) D.-P. Song, C. Li, W. Li, J. J. Watkins, *ACS Nano* **2016**, *10*, 1216; d) Q. Yuan, M. Zhang, D. Wang, Y. Lv, S. Liu, H.-Y. Mi, J. Han, C. Liu, C. Shen, *ACS Appl. Mater. Interfaces* **2024**, *16*, 29141.
- [26] a) H. S. Lee, T. S. Shim, H. Hwang, S.-M. Yang, S.-H. Kim, *Chem. Mater.* **2013**, *25*, 2684; b) G. H. Lee, S. H. Han, J. B. Kim, J. H. Kim, J. M. Lee, S.-H. Kim, *Chem. Mater.* **2019**, *31*, 8154; c) Q. Fan, Z. Li, Y. Li, A. Gao, Y. Zhao, D. Yang, C. Zhu, T. V. Brinzari, G. Xu, L. Pan, L. T. Vuong, Y. Yin, *J. Am. Chem. Soc.* **2023**, *145*, 28191; d) F. Meng, B. Ju, Z. Wang, R. Han, Y. Zhang, S. Zhang, P. Wu, B. Tang, *J. Am. Chem. Soc.* **2022**, *144*, 7610.
- [27] Y. Wu, Y. Wang, S. Zhang, S. Wu, *ACS Nano* **2021**, *15*, 15720.
- [28] Q. Fu, H. Zhu, J. Ge, *Adv. Funct. Mater.* **2018**, *28*, 1804628.
- [29] a) X. Su, Y. Jiang, X. Sun, S. Wu, B. Tang, W. Niu, S. Zhang, *Nanoscale* **2017**, *9*, 17877; b) D. Wang, J. Li, X. Sun, J. Hu, X. Tan, Q. Jia, J. Liu, X. Zhang, G. Wu, X. Wang, *J. Colloid Interface Sci.* **2024**, *654*, 581; c) Z. Chen, H. Jia, Z. Liu, Y. Chen, J. Wei, *Chem. Eng. J.* **2024**, *480*, 148185.
- [30] C. Wu, Q. Fang, J. Li, X. Su, *J. Mater. Chem. C* **2024**, *12*, 6952.
- [31] a) Y. Hu, Z. Tian, D. Ma, C. Qi, D. Yang, S. Huang, *Adv. Colloid Interface Sci.* **2024**, *324*, 103089; b) Y. Hu, C. Qi, D. Ma, D. Yang, S. Huang, *Nat.*

- Commun.* **2024**, *15*, 5643; c) S. Yu, D. Ma, C. Qi, D. Yang, S. Huang, *Adv. Funct. Mater.* **2024**, 2411670.
- [32] a) H. Li, P. Wu, G. Zhao, J. Guo, C. Wang, *J. Colloid Interface Sci.* **2021**, *584*, 145; b) M. Li, B. Peng, Q. Lyu, X. Chen, Z. Hu, X. Zhang, B. Xiong, L. Zhang, J. Zhu, *Nat. Commun.* **2024**, *15*, 1874.
- [33] Q. Guo, S. Chen, H. Li, X. Wang, J. He, J. Chu, J. Guo, C. Wang, *Chem. Eng. J.* **2024**, *488*, 150969.
- [34] X. Zhang, Q. Lyu, X. Chen, M. Li, L. Zhang, J. Zhu, *ACS Appl. Mater. Interfaces* **2024**, *16*, 15308.
- [35] J. He, Y. Zang, H. Li, J. Guo, C. Wang, *Chem. Eng. J.* **2024**, *497*, 154838.